© 2026 IEEE. Personal use of this material is permitted. Permission from IEEE must be obtained for all other uses, in any current or future media, including reprinting/republishing this material for advertising or promotional purposes, creating new collective works, for resale or redistribution to servers or lists, or reuse of any copyrighted component of this work in other works. This is the author's accepted manuscript of an article published in IEEE Journal of Biomedical and Health Informatics. The final published version is available at https://doi.org/10.1109/JBHI.2026.3745760. L. Lin et al., "EEG Edge-Centric Dynamics Reveal Distinct Post-Stroke Somatosensory Network Responses to Vibratory and Electrical Stimulation," IEEE J. Biomed. Health Inform., pp. 1–12, 2026, doi: 10.1109/JBHI.2026.3745760.

EEG Edge-Centric Dynamics Reveal Distinct Post-Stroke Somatosensory Network Responses to Vibratory and Electrical Stimulation

Legeng Lin, *Member, IEEE*, Jiahui Liao, Yanhuan Huang, Wanyi Qing, Fuqiang Ye, Wei Rong, Waiming Li, Jiao Jiao, Xiaoling Hu, *Senior Member, IEEE*, and Ting Ma, *Senior Member, IEEE*

***Abstract*—Stroke-induced somatosensory deficits disrupt sensorimotor integration (SMI) and limit motor recovery, yet the immediate network-level effects of different somatosensory interventions remain unclear, hindering patient-specific rehabilitation planning. We propose an informatics framework based on edge-centric dynamic connectivity (ECDC) to characterize transient, whole-brain EEG network responses to sensory-level focal vibratory stimulation (FVS) and neuromuscular electrical stimulation (NMES). We analyzed EEG recordings from 15 chronic stroke participants and 15 healthy controls during forearm stimulation and quantified temporal network dynamics, spectral network organization, and interhemispheric interactions from instantaneous overlapping functional networks. Compared with NMES, FVS in stroke participants induced a distinct neurophysiological profile, including (i) shorter global theta-network latency, suggesting faster attentional engagement; (ii) higher contralesional alpha-network diversity, indicating enhanced somatosensory recruitment; and (iii) reduced theta-alpha phase-amplitude coupling, reflecting decoupled interhemispheric interactions that may support adaptive reorganization. These findings provide interpretable network signatures for differentiating stimulation-specific brain responses and suggest a data-driven route toward personalized SMI rehabilitation.**

***Index Terms*— Edge-centric brain network, focal vibratory stimulation, functional connectivity, neuromodulation, somatosensory processing, stroke.**

I. Introduction

STROKE is a leading cause of long-term disability; over half of survivors experience somatosensory deficits [1]. These deficits disrupt the brain's somatosensory network and impair sensorimotor integration (SMI), which worsens motor dysfunction and hinders recovery [2]. SMI uses somatosensory input (e.g. tactile and proprioceptive feedback) to shape movement in a closed loop [3] and to enable motor relearning via neuroplasticity after stroke [4]. After stroke, ascending feedback from a target muscle can become overwhelmed by feedback from compensatory muscles [5], [6]. This disrupted SMI may promote maladaptive neuroplasticity, leading to abnormal movement patterns, muscular compensation and long-term learned disuse [7], [8]. Therefore, restoring coordinated movement requires reconstructing closed-loop SMI by reintegrating targeted somatosensory input during rehabilitation [3], [4], [7]. Effective strategies must thus supplement traditional motor training with somatosensory stimulation to facilitate functional recovery [2], [9].

Combining somatosensory priming of targeted muscles with routine limb therapy improves outcomes more than therapy alone, due to enhanced ascending sensory facilitation [7], [10]. In practice, priming is typically delivered non-invasively via neuromuscular electrical stimulation (NMES) or focal vibratory stimulation (FVS) [10]. Both modalities, when integrated with

This work was supported by National Key Research and Development Program, China (2025YFF0517803), the University Grants Committee Research Grants Council, Hong Kong (GRF15207120, GRF15218324 and GRF15215025); the Innovation and Technology Fund (ITT/012/23GP and ITS/011/23); the Strategic Topics Grant (STG1/M-401/24-N); and The Hong Kong Polytechnic University (4-CEB2); National Natural Science Foundation of China (62276081); Guangdong S&T Programme, China (2025B0101130004); Shenzhen Science and Technology Program, China (JCYJ20250604145427037, CJGJZD20230724093959002). *(Legeng Lin and Jiahui Liao, co-first authors, contributed equally to this work.) (Corresponding authors: Xiaoling Hu; Ting Ma.)*

Legeng Lin, Yanhuan Huang, Wanyi Qing, Fuqiang Ye, Wei Rong, Waiming Li, and Xiaoling Hu are with the Department of Biomedical Engineering, The Hong Kong Polytechnic University, Hong Kong SAR 999077, China, and with the Research Institute for Smart Ageing (RISA), The Hong Kong Polytechnic University, Hong Kong SAR 999077, China; Xiaoling Hu is also with the Research Institute for Sports Science and Technology (RISports), The Hong Kong Polytechnic University, Hong Kong SAR 999077, China, and the Joint Research Centre for Biosensing and Precision Theranostics, The Hong Kong Polytechnic University, Hong Kong SAR 999077, China (e-mail: logan.lin@polyu.edu.hk; yanhuan731.huang@polyu.edu.hk; wanyi.qing@connect.polyu.hk; fuqiang.ye@connect.polyu.hk; rongwei@live.com; deo-li@hotmail.com; xiaoling.hu@polyu.edu.hk).

Jiahui Liao is with the School of Information Science and Technology, Harbin Institute of Technology (Shenzhen), Shenzhen 518055, China (e-mail: 23B952013@stu.hit.edu.cn).

Jiao Jiao is with the Department of Sport, Physical Education and Health, Hong Kong Baptist University, Hong Kong SAR 999077, China (e-mail: jojojiao@hkbu.edu.hk).

Ting Ma is with the School of Biomedical Engineering, Harbin Institute of Technology (Shenzhen), Shenzhen 518055, China (e-mail: tma@hit.edu.cn).

This article has supplementary material provided by the authors.

Color versions of one or more of the figures in this article are available online at http://ieeexplore.ieee.org

standard or robotic training, promote motor recovery in chronic stroke [9], [11], [12]. However, their contributions differ based on distinct physiological mechanisms.

NMES, the conventional benchmark, is usually applied at motor-level intensity to cause muscle contraction through the depolarization of motor nerves or muscle fibers [13], enhancing force and preventing atrophy while also providing somatosensory input [12], [14], [15], [16]. At lower, sensory-level intensities, NMES depolarizes sensory neurons without causing contraction [17], which can improve proprioception and reduce compensatory muscle synergies [14]. A key drawback is that NMES broadly activates diverse sensory receptors associated with pain. Prolonged use may also increase hypertonia and induce muscle fatigue [7], [18].

In contrast, FVS primarily activates muscle mechanoreceptors. It facilitates somatosensory input comfortably without exacerbating spasticity [19], [20]. By deforming muscle spindles in a manner analogous to manual massage, FVS activates primary afferent endings (i.e. Ia afferents), which can in turn enhance proprioception, suppress antagonist co-contraction [17], [20] and alleviate post-stroke spasticity [11]. The rehabilitation benefits of both FVS and NMES require the accumulation of immediate neuromodulatory effects to drive long-term neuroplasticity. Consequently, understanding these immediate neuromodulatory effects is essential for optimizing their application in SMI stroke rehabilitation.

Electroencephalography (EEG) provides superior temporal resolution compared to other neuroimaging techniques, a crucial advantage for analysing the instantaneous neural dynamics of somatosensory processing [18], [19]. At the signal level, EEG studies show that both FVS and NMES rapidly activate the sensorimotor cortex [18], [19]. For stroke survivors, FVS appears especially effective in triggering transient, involuntary attention responses [19]. This signal-level profile suggests FVS is better suited for somatosensory priming during SMI rehabilitation, because effective priming requires quickly focusing attention on target muscles to integrate sensation with motor execution in the cortex, thereby promoting SMI restructuring via Hebbian neuroplasticity [21]. NMES, on the other hand, primarily fosters cortical responses of the targeted muscles in the contralesional motor cortex more strongly than FVS [19]. This difference suggests that FVS and NMES may operate through distinct mechanisms to adjust interhemispheric balance as well.

Efficient somatosensory processing relies on brain-wide networks rather than isolated signal-level regions; thus, it is critical to understand how FVS versus NMES rapidly reshape these networks after stroke. Functional connectivity (FC) analyses have greatly advanced our understanding of somatosensory networks in chronic stroke [14], [22]. Standard, node-centric FC (nFC) methods characterize the communication strength between brain regions. Studies using nFC show that both FVS and NMES modulate brain connectivity. For example, sensory-level NMES boosts fronto-parietal nFC, which improves the accuracy and stability of motor imagery tasks to aid recovery [14]. FVS, meanwhile, strengthens nFC between the primary somatosensory (S1) and motor cortices, potentially supporting post-stroke motor relearning [23]. These findings demonstrate a rehabilitative mechanism via modulating brain network. However, standard nFC methods fail to capture the brain's transient, dynamic network properties within regionally overlapping functional modules. This limitation stems from inherent assumptions of stationarity, low temporal resolution and mutually exclusive module partitions [24].

Edge-centric network analysis overcomes these limitations. This approach employs edge time series (eTS) and edge FC (eFC), typically applied to the blood-oxygen-level-dependent (BOLD) signal of functional MRI but easily extended to EEG data [24]. Mathematically, nFC correlations are the average of instantaneous co-fluctuations between node pairs. By omitting the final averaging step and keeping the raw co-fluctuation products, edge-centric analysis generates eTS and eFC that exactly decompose nFC into frame-by-frame dynamics. This preserves temporal resolution, avoids arbitrary windowing and allows connections themselves to be treated as fundamental units, enabling overlapping community detection and richer characterization of brain organization. It uniquely captures the instantaneous, dynamic, overlapping functional network patterns of sensorimotor and attention systems that node-centric approaches fail to reveal [24], [25]. Consequently, edge-centric analysis is a precise tool for revealing the dynamic network reconfigurations of somatosensory processing [26]. Edge time series and edge-centric connectivity approaches have been applied to EEG and MEG data previously [27], [28], but to our knowledge limited research has employed ECDC to compare FVS versus NMES in stroke.

This work aims to provide mechanistic insights into the application of FVS in SMI-focused stroke rehabilitation. To this end, in this single-session, cross-sectional study of chronic stroke survivors and unimpaired controls, we applied an edge-centric dynamic connectivity (ECDC) framework to analyze network dynamics at the level of connections (edges) in addition to nodes. With this approach, we compared the immediate effects of FVS versus NMES on network properties. Building on previous signal-level evidence [19], we hypothesized that FVS and NMES engage distinct network reconfiguration patterns, with faster engagement of attention-related theta circuits and enhanced recruitment of contralesional alpha networks expected under FVS, and stronger driving of the ipsilesional alpha network and more pronounced cortical responses of the targeted muscles in the contralesional motor cortex expected under NMES.

II. Methods

We used the ECDC framework (Fig. 1) to investigate how FVS immediately modulates the somatosensory network after stroke compared to sensory-level NMES. Our EEG analyses aimed to reveal temporal dynamics, spectral network properties and interhemispheric functional interactions. After preprocessing, we calculated eTS to find transient network



Fig. 1. Workflow of ECDC analysis framework for comparison of immediate network configuration between sensory-level FVS and NMES after stroke. **(a)** Experiment setup in the collection of raw EEG dataset. **(b)** The eTS construction based on the phase difference of EEG data between two nodes (channels). **(c)** Root mean square (RMS) of whole-brain eTS (i.e. eRMS). The time periods of significant cortical network responses induced by stimulations are detected by cluster-based permutation test ($P < 0.05$) on eRMS in each group compared to the baseline, defined as the time of interests (TOIs). EEG data corresponding to TOIs are intercepted for further node- and edge-centric network and phase–amplitude coupling (PAC) analysis. **(d)** Node-centric network property analysis. RH in the stroke group was the ipsilesional hemisphere. Patterns included global efficiency (GE), local efficiency (LE), connection density K, node strength (NS) and brain asymmetry index (BAI). **(e)** Edge-centric network property analysis. **(f)** Cross-frequency PAC analysis.

patterns and identified a time of interest (TOI) based on significant eTS responses. Within this TOI, we then analyzed spectral networks from two angles: Regional (node-centric) connectivity and higher-order interactions within overlapping (edge-centric) modules. Finally, we measured cross-frequency phase–amplitude coupling (PAC) to assess interhemispheric interactions. Together, this multistage, multiscale approach captured how FVS reconfigures post-stroke somatosensory processing versus NMES.

A. EEG dataset and preprocessing

This study involved secondary analyses of published EEG data [19], approved by the Hong Kong Polytechnic University Ethics Committee (HSEARS20210320003). The dataset captured transient cortical responses to transcutaneously applied sensory-level stimulation (FVS at 1.9 G; NMES at the median intensity between perceptual and motor thresholds) on participants' forearm muscles of the non-dominant upper limbs (i.e. affected side for stroke group and left side for the control group), designed to evoke somatosensory responses (Fig. 1A). Fifteen participants with chronic stroke and 15 unimpaired controls were recruited, with inclusion/exclusion criteria, demographic data, clinical scores for stroke participants, experimental setup and detailed protocols available in the Supplementary methods and Supplementary Table S1 and S2.

Whole-brain EEG data were recorded at 1000 Hz during stimulation, with stimulation onset marked for each epoch to enable precise time-course analysis. EEG preprocessing was performed using EEGLAB toolbox and included the following steps: (i) digital band-pass filtering (1–100 Hz) and 50 Hz notch filtering via a fourth-order Butterworth filter; (ii) re-referencing by linked mastoids and independent component analysis (ICA), performed using the extended infomax algorithm (pop_runica, EEGLAB); components were classified using ICLabel [29], with components having ≥80% probability for any non-brain category (eye, muscle, heart, line noise, channel noise) automatically flagged and then confirmed by visual inspection of their scalp maps, time courses, and spectra; on average, 11.09±5.47 components were removed per participant dataset (healthy controls: 10.87±5.33; stroke group: 11.30±5.63); (iii) visual artifact removal and interpolation of bad channels; (iv) down-sampling to 250 Hz; and (v) epoch extraction based on onset markers, each encompassing a 5-second baseline and 10-second stimulation phase (i.e. [-5, 10] s). For participants with left hemisphere lesions, EEG electrode positions were flipped along the mid-sagittal plane to standardize the ipsilesional hemisphere to the right side across all stroke participants [19]. In this study, a total of 150 stimulation epochs were further analyzed in ECDC framework for each stimulation modality in each group.

B. Temporal dynamics and TOI detection based on eTS

We derived eTS to investigate transient temporal network patterns and identify time of interest (TOI) by locating significant responses in the eTS compared with baseline. The excellent temporal resolution of eTS provides a unique tool to investigate the transient dynamics of brain network in response to sensory stimuli. It captures the phase difference between two nodes (channels) of EEG to generate eTS as shown in Fig. 1B, inspired by the facilitation of phase-based intrinsic coupling modes in communication between separate neuronal circuits during stimuli [30].

To be specific, the instantaneous phase of each channel was first computed using the Hilbert transform. The eTS for each channel pair $\{i, j\}$ was then computed using the cosine of the phase difference between channel pair:

$$eTS_{ij}(t) = \cos\left(\varphi_i(t) - \varphi_j(t)\right) \quad (1)$$

where $\varphi_i(t)$ and $\varphi_j(t)$ denote the unwrapped phase of channels i and j at time t. This transformation provided a continuous measure of phase synchronization, where values close to one indicated strong in-phase coupling, while values close to negative one suggest anti-phase synchronization.

Our analysis began with the theta rhythm (4-8 Hz), a key neural correlate of attention capture and sensory gating for new information [31]. This initial engagement is fundamental to the integration of somatosensory stimuli for sensorimotor processing, reflected by the alpha rhythm (8-13 Hz) [32], and the processing of motor commands and functions, mainly reflected by the beta rhythm (13-30 Hz) in pre-motor and primary sensorimotor cortex (S1–M1) regions [22]. Inspired by these studies, eTS for theta, alpha and beta bands were calculated here. Other frequency bands were not included for the following reasons. Gamma (>30 Hz) was not analyzed because in our prior dataset-level analysis, gamma-band responses showed no significant differences between FVS and NMES in the stroke group [19]. Delta (1–4 Hz) was not analyzed, because the ~1 s TOI yields very few delta cycles, making phase-based metrics statistically unreliable, and delta is also susceptible to residual ocular contamination.

The high-amplitude co-fluctuations in the BOLD signals, defined as the brain-wide 'events', help to explain the system-level organization and coupling structure of the brain [25]. Inspired by this, we have derived the brain-wide 'events' in the electrophysiological signals to precisely locate the time periods of the brain in response to the sensory stimulations. At each time point, the overall magnitude of whole-brain instantaneous phase coupling was quantified as the root mean square (RMS) across all phase-based eTS values, referred to as eRMS (Fig. 1B). The TOI was defined as the time window during which eRMS was significantly different from the baseline, meaning significant cortical network responses to stimuli (Fig.1C), and was used for subsequent analyses.

C. Node-centric regional network property analysis

We first performed node-centric analysis within TOIs (Fig. 1D) to characterize the specific contributions of individual brain regions and their connectivity patterns to the overall network response during the identified TOIs. Phase locking value (PLV), one of the most classic methods for weighted undirected nFC calculation [33], was utilized in this study as follows:

$$PLV = \frac{1}{T}\left|\sum_{t=1}^{T} \exp\left(j\Delta\varphi_{ij}(t)\right)\right| \quad (2)$$

where T indicated the total time points, $\Delta\varphi_{ij}(t)$ indicated the phase difference between $\varphi_i(t)$ and $\varphi_j(t)$. The value of PLV ranged from zero to one, and one indicated the synchronization between $\varphi_i(t)$ and $\varphi_j(t)$. The significant nFC (Sig-nFC) in response to stimuli was determined by significant connections in PLV_{TOI} with respect to $PLV_{baseline}$ [34].

The node-centric graph-theoretic indices based on Sig-nFC in response to stimulation were further calculated at three scales as follows: (i) large-scale indices quantified the global properties of the functional brain network by describing the efficient communication of the entire brain, including global efficiency (GE) and local efficiency (LE); (ii) intermediate-scale indices measured the information interaction between/within hemispheres, including network connection density of inter-hemisphere (K-inter) and density of intra-left/right hemisphere (K-LH/RH); and (iii) small-scale indices analyzed spatial network distribution and laterality based on node strength (NS) and brain asymmetry index (BAI). The calculation formula for each measure and additional explanation [35] were summarized in Supplementary Table S3.

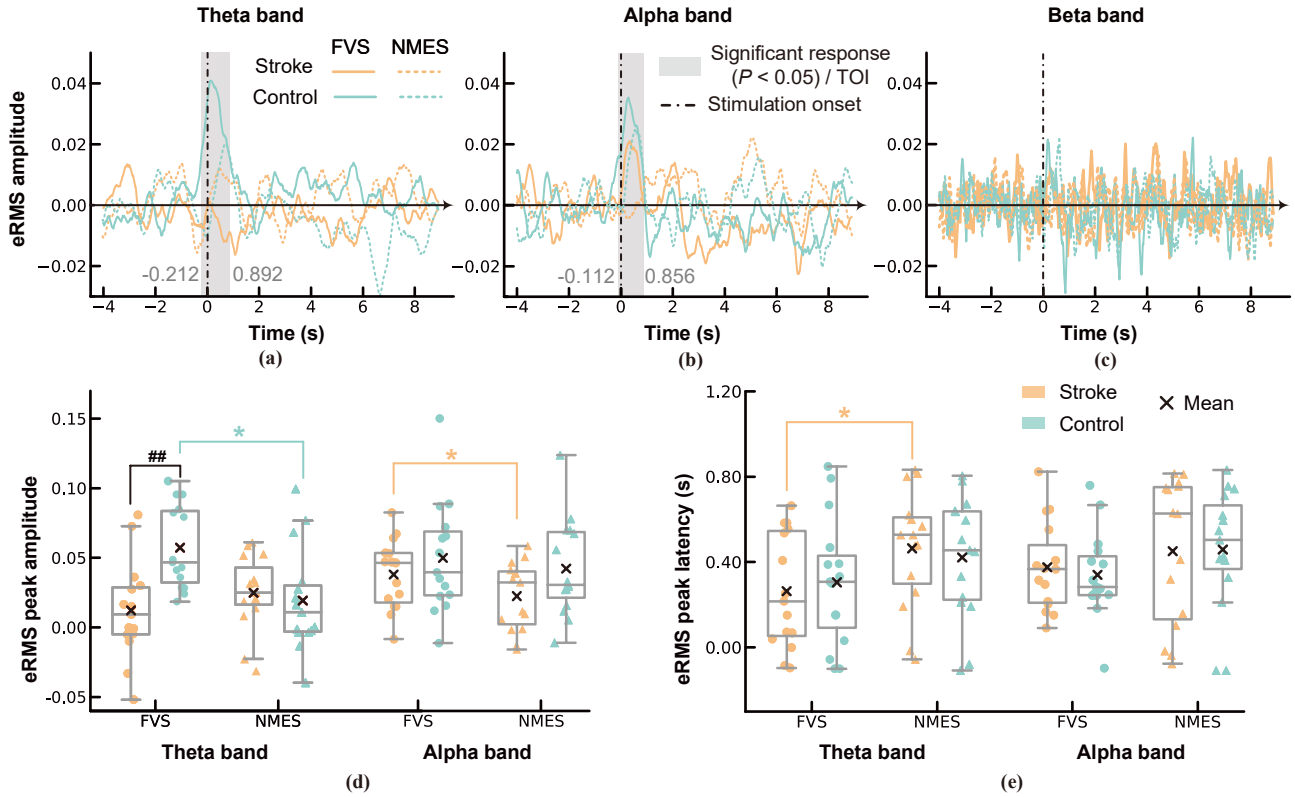


Fig. 2. eRMS averaged across participants showing the immediate cortical network responses to stimulation in the theta **(a)**, alpha **(b)** and beta **(c)** bands. The vertical black lines at 0 s indicate stimulations onset. Light grey shading indicates significant eRMS peak, i.e. time of interest (TOI), where the response was significantly different from the baseline period (-5 to 0 s) ($P < 0.05$, cluster-based permutation test). Comparisons of eRMS peak amplitude **(d)** and latency **(e)** in the theta and alpha bands. Significant inter- and intra-group differences are indicated by "#" and "*", respectively (#/* for $P < 0.05$, ## for $P < 0.01$).

D. Edge-centric overlapping network property analysis

To capture higher-order interaction and organization within the overlapping functional network modules that are not accessible through node-centric connectivity alone, we further employed edge-centric network property analysis (Fig.1E). Specifically, eFC allows us to investigate the statistical dependencies between the functional connections themselves (i.e. pairs of edges), rather than between pairs of nodes, revealing richer details about how network interactions co-vary and form naturally overlapping community [24], [25]. Let $e_{ij} = [eTS_{ij}(1), \ldots, eTS_{ij}(T)]$ and $e_{uv} = [eTS_{uv}(1), \ldots, eTS_{uv}(T)]$ be the time series for edges (channel pairs) $\{i, j\}$ and $\{u, v\}$, respectively. eFC was calculated as follows:

$$eFC_{ij,uv} = \frac{\sum_{t=1}^{T} e_{ij}(t) \cdot e_{uv}(t)}{\sqrt{\sum_{t=1}^{T} e_{ij}(t)^2}\sqrt{\sum_{t=1}^{T} e_{uv}(t)^2}} \qquad (3)$$

eFC matrices of dimension (M, M) were much larger than nFC matrices. To reduce its dimensionality, we concatenated eFC for each stimulation modality in each group, and then performed uniform manifold approximation and projection (UMAP), generating a common embedding space where each scatter represented an eFC of a pair of edges. Then K-means clustering algorithm, with varied number of communities, k, from 20 to 40, was applied on the embeddings to generate group-representative edge communities [24], [36]. The clustering algorithm partitioned edges into non-overlapping clusters and every edge $\{i, j\}$, was assigned to one of the k clusters. Participation in cluster c of node i was calculated as follows:

$$p_{ic} = \frac{1}{N-1}\sum_{j \neq i} \delta(g_{ij}, c) \qquad (4)$$

where $g_{ij} \in \{1,\ldots,k\}$ was the cluster assignment of the edge linking node i and j, and $\delta(x, y)$ is the Kronecker delta, whose value is one if x=y, and zero otherwise. By definition, $\sum_x p_{ic} = 1$, and we can treat the vector $p_i = [p_{i1}, \ldots, p_{ik}]$ as a probability distribution. The entropy of this distribution measures the level of edge community overlaps for given regions. To investigate the communication patterns at the hemispheric level, the normalized entropy (NE) was calculated for the inter- and intra-hemispheric edges respectively as follows:

$$NE_i = -\sum_{c} p_{ic} \log_2 p_{ic} \qquad (5)$$

The values of NE close to 0 indicate that edges of the specific regions were concentrated among a small number of edge communities, whereas values close to 1 indicated that edges were uniformly distributed over edge communities. As the number of cluster k set from 20 to 40, NE for each scheme in each group had 20 samples for further intra- and inter-group statistical comparison.

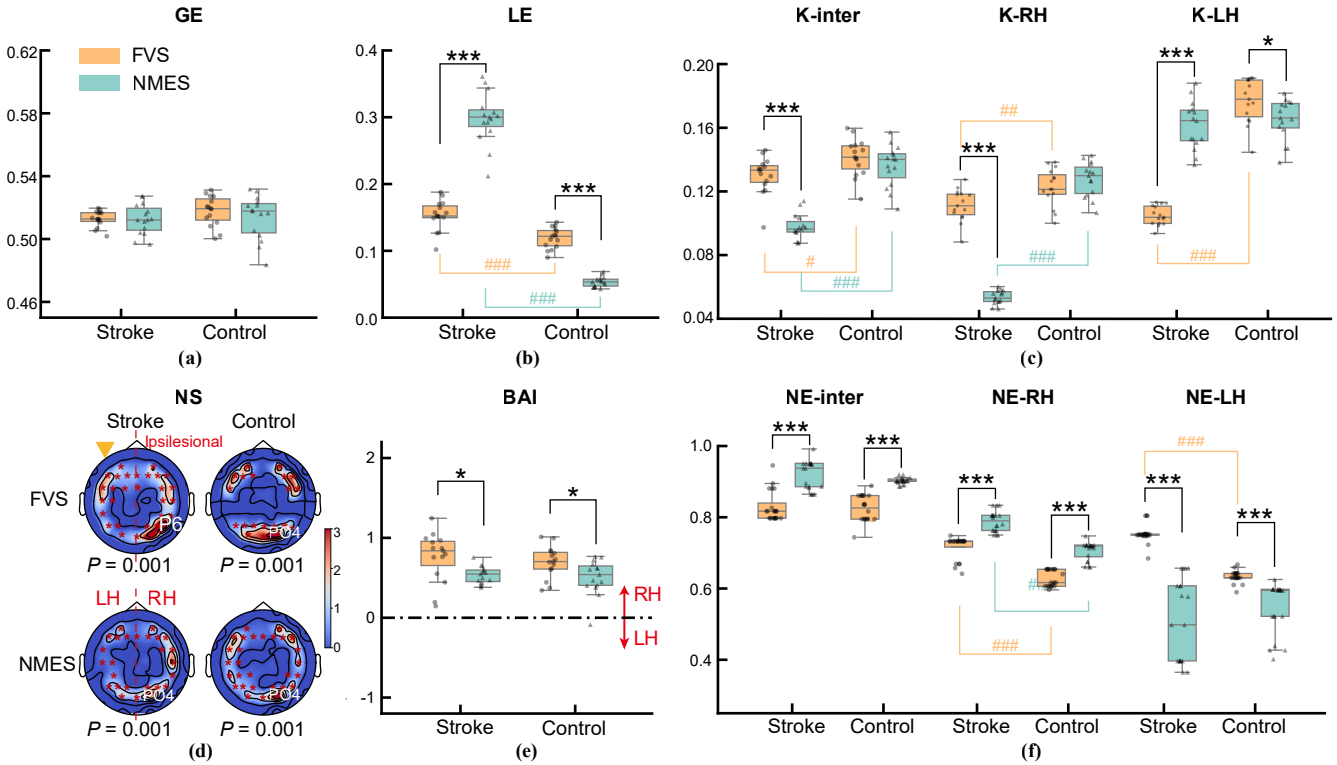


Fig. 3. Theta-band network responses within time of interest (TOI). Large-scale global efficiency (GE) **(a)** and Local efficiency (LE) **(b)**. **(c)** Intermediate-scale connection density K between hemisphere (K-inter), within the right hemisphere (K-RH) and within the left hemisphere (K-LH). **(d)** Topographies of small-scale node strength (NS). Significant nodes compared to baseline were marked in red. RH in the stroke group was the ipsilesional hemisphere. **(e)** Brain asymmetry index (BAI) quantifying hemispheric lateralization of NS. **(f)** Intermediate-scale connection diversity measured by normalized entropy (NE) between hemisphere (NE-inter), within the right hemisphere (NE-RH) and within the left hemisphere (NE-LH). Significant inter- and intra-group differences are indicated by "#" and "*", respectively (#/* for $P < 0.05$, ##/** for $P < 0.01$, ###/*** for $P < 0.001$).

E. Inter-hemispheric functional interaction analysis by cross-frequency PAC

Cross-frequency PAC, a widely used measure that quantifies the extent to which the *phase* of low-frequency oscillations modulates the *amplitude* of higher-frequency oscillations [37], was used to reflect the potential mechanism for cross-frequency neural communication between/within hemispheres. We employed the modulation index (MI), a robust method to quantify PAC with high signal-to-noise ratio, particularly in short data epochs [38]. MI is calculated as follows by comparing the amplitude-phase distribution (P) against the null hypothesis of a uniformly amplitude-phase distribution (Q).

$$MI = \frac{D(P,Q)}{\log(N_{bins})} = \frac{\sum_{j=1}^{N_{bins}} P(j) \cdot \log\left(\frac{P(j)}{Q(j)}\right)}{\log(N_{bins})} \qquad (6)$$

where N_{bins} is the number of discrete bins of the theta phase cycle and set to 18 following [38]. $D(P, Q)$ is the Kullback-Leibler distance, related to Shannon's entropy. The calculation was performed on the EEG data within TOIs for each participant. The channel-wise rhythms were extracted to compute a full channel-by-channel PAC matrix, where each entry represents the coupling strength between the 'phase' of low-frequency oscillations in a source channel and the 'amplitude' of higher-frequency oscillations in a target channel. From this complete matrix, summary metrics were derived by averaging the PAC values across relevant channel pairs in specified hemispheres.

F. Statistical analysis

The statistical analysis was conducted for eRMS, node-, edge-centric and cross-frequency PAC measures. Non-parametric cluster-based permutation test (5000 permutations) with respect to the baseline was utilized to detect TOI in eRMS, significant connections in nFC (i.e. Sig-nFC) and significant nodes in NS topography, respectively. Shapiro–Wilk normality test was first performed for the amplitude and latency of eRMS peaks, the node-centric and edge-centric measures and the cross-frequency PAC. For normally distributed results ($P > 0.05$), paired and independent t-tests were applied to the respective intra-group or inter-group comparisons between stimulation modalities or cohort groups. For non-normally distributed indices ($P < 0.05$), Wilcoxon signed-rank tests were conducted for intra-group comparison, and Mann–Whitney U-tests for inter-group comparison. The significance level in this study was set at $P < 0.05$, with $P < 0.01$ and 0.001 also reported.

To further examine the potential associations between the ECDC network metrics and clinical function, Spearman rank correlations were performed within the stroke group (n=15). Specifically, the network metrics examined in this study were correlated with the current FMA-UE scores to assess motor function, whereas the NE metrics in the theta and alpha bands

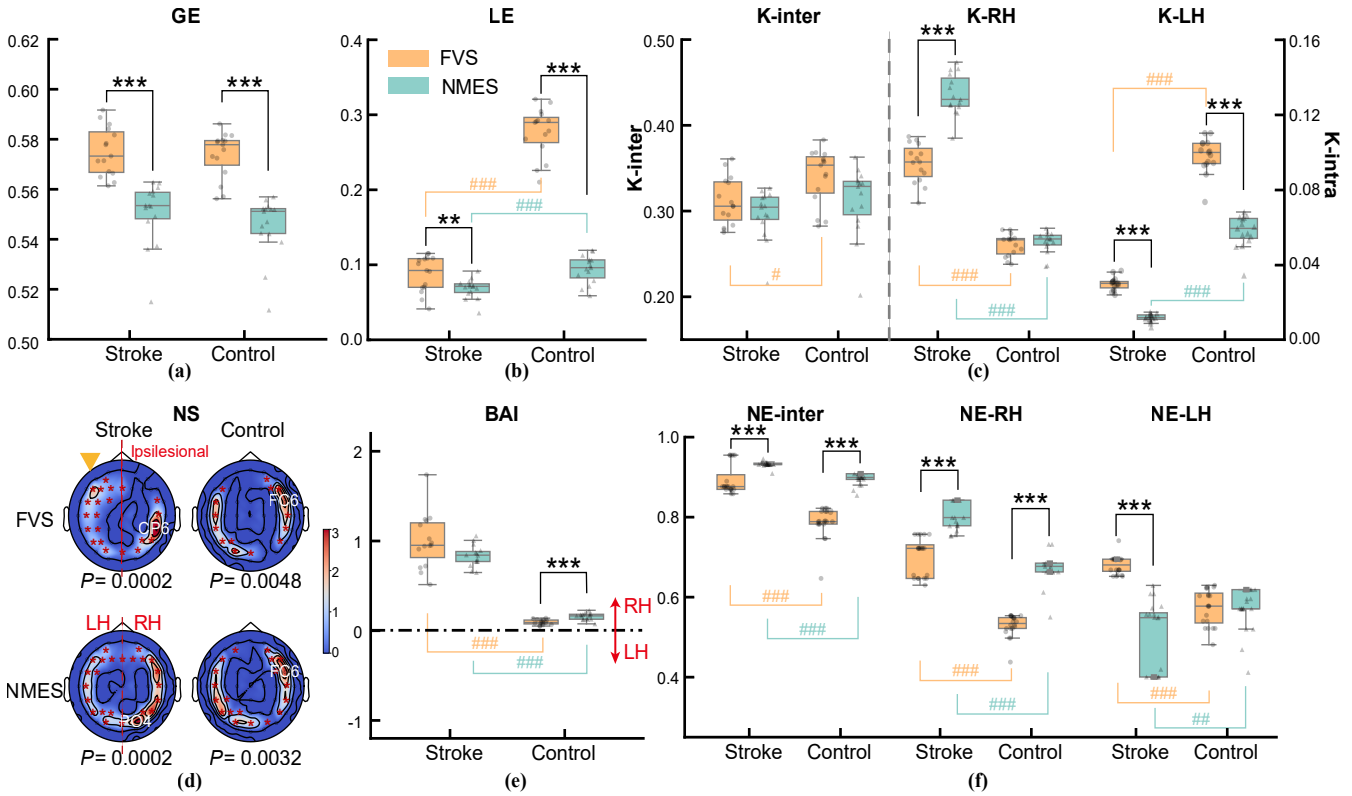


Fig. 4. Alpha-band network responses within time of interest (TOI). Large-scale GE **(a)** and LE **(b)**. **(c)** Intermediate-scale connection density measured by K-inter, K-RH and K-LH. **(d)** Topographies of small-scale NS. Significant nodes compared to baseline were marked in red. RH in the stroke group was the ipsilesional hemisphere. **(e)** BAI quantifying hemispheric lateralization of NS. **(f)** Intermediate-scale connection diversity measured by NE-inter, NE-RH and NE-LH. Significant inter- and intra-group differences are indicated by "#" and "*", respectively (#/* for $P < 0.05$,

were correlated with the Semmes–Weinstein monofilament scores on the affected side to assess sensory impairment. Correlation coefficients were tested against zero using a permutation approach (10,000 permutations), and false discovery rate (FDR) correction (Benjamini–Hochberg) was applied separately within each set of tested correlations.

III. Results

A. Temporal dynamics and detected TOIs

The global cortical network response to sensory stimulation was first characterized by analysing the RMS of eTS (eRMS) across the theta, alpha and beta bands (Fig. 2, Supplementary Table S4). Significant stimulus-locked eRMS peaks (TOIs for subsequent analysis) were detected in the theta and alpha bands ($P < 0.05$, cluster-based permutation test). The TOI for the theta band was identified as -0.212 to 0.892 s, and for the alpha band, -0.112 to 0.856 s. No significant response was observed in the beta band. The slight negative onsets of the theta and alpha TOIs (−0.212 and −0.112 s, respectively) reflect the temporal extent of the cluster-based permutation results [39], which can extend a significant cluster slightly across stimulus onset.

Based on these initial findings, all subsequent analyses were focused on the identified TOIs within the theta and alpha bands. During FVS, the stroke group exhibited a significantly lower peak amplitude in the theta band compared to the control group (Fig. 2D). Within the control group, FVS induced a significantly higher peak amplitude than NMES in the theta band (Fig. 2D). Within the stroke group, FVS demonstrated a significantly higher alpha-band peak amplitude (Fig. 2D) and a significantly shorter theta-band peak latency (Fig. 2E) compared to NMES.

B. Node- and edge-centric spectral network properties

Significant differences in theta-band network properties within TOI were observed between groups and stimuli (Fig. 3, Supplementary Table S5). No significant difference in GE was detected (Fig. 3A), whereas LE was significantly elevated in stroke participants relative to healthy controls ($P < 0.001$; Fig. 3B). Within the stroke cohort, LE was further increased under NMES compared to FVS ($P < 0.001$). Almost all connection density Ks were found to be significantly lower in stroke participants than in controls ($P < 0.05$, Fig. 3C). Notably, NMES further reduced K-inter/RH, whereas FVS further decreased K-LH in stroke participants ($P < 0.001$). At the node level (Fig. 3D), the NS topography showed bilateral network response with concentration in the right parietal region (P6, PO4). This hemispheric bias was quantified by BAI, which revealed that FVS induced a significantly greater lateralization toward the RH compared to NMES ($P < 0.05$, Fig. 3E). Regarding connection diversity quantified by NE, FVS significantly increased NE-LH while decreased NE-inter/RH compared to NMES ($P < 0.001$, Fig. 3F), in both the stroke and control groups.

Significant differences in alpha-band network properties within TOI were observed between groups and stimuli (Fig. 4,

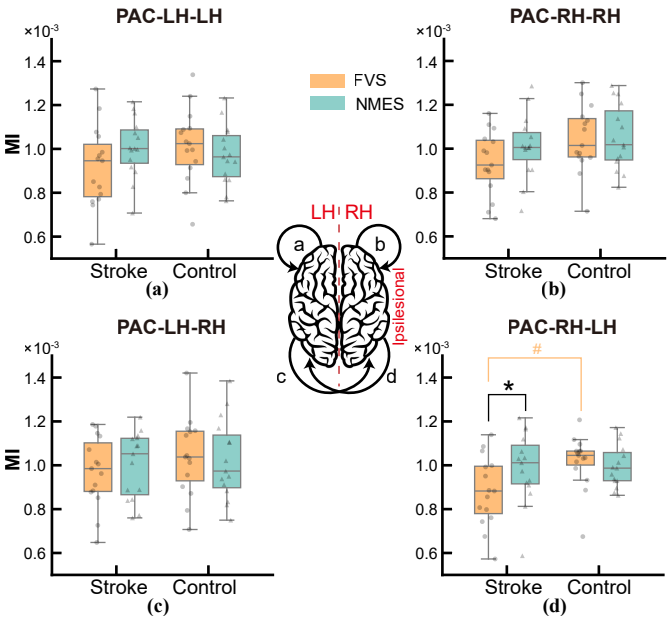


Fig. 5. Hemispheric cross-frequency phase–amplitude coupling (PAC) from theta phase to alpha amplitude, measured by modulation index (MI). **(a)** Intra-hemispheric PAC within LH (PAC-LH-LH), **(b)** Intra-hemispheric PAC within RH (PAC-RH-RH). **(c)** Inter-hemispheric PAC from LH to RH (PAC-LH-RH). **(d)** Inter-hemispheric PAC from RH to LH (PAC-RH-LH). Significant inter- and intra-group differences are indicated by "#" and "*", respectively (#/* for $P < 0.05$).

Supplementary Table S6). FVS yielded significantly higher GE and LE than NMES in each group ($P < 0.01$, Fig. 4A and B). Stroke group showed significantly impaired LE compared to controls ($P < 0.001$). Connection density was found to be significantly higher in K-RH and lower in K-LH of stroke participants than those of controls ($P < 0.001$, Fig. 4C). Notably, FVS reduced K-RH but enhanced K-LH in stroke participants compared with NMES ($P < 0.001$). At the node level (Fig. 4D), the NS topography showed bilateral network response with concentration in the right frontal-central–parietal region (FC6, CP6, PO4). BAI revealed that stroke group had a significantly greater lateralization toward the RH compared to the controls with bilateral balance ($P < 0.001$, Fig. 4E). All connection diversity NEs were found to be significantly higher in stroke participants than in controls ($P < 0.001$, Fig. 4F). FVS significantly increased NE-LH while decreasing NE-inter/RH compared to NMES, especially in the stroke group ($P < 0.001$).

C. Hemispheric cross-frequency functional interactions

The analysis of cross-frequency PAC revealed key differences primarily in the hemispheric coupling from the theta phase in RH to the alpha amplitude in LH (PAC-RH-LH, Fig. 5D, Supplementary Table S7). The primary inter-group difference was observed under FVS, where the stroke group exhibited significantly lower PAC than the control group ($P = 0.023$). The intra-group difference was observed within the stroke group, where FVS induced significantly lower PAC compared to NMES ($P = 0.021$). No significant differences were found for any other PAC measures (PAC-RH-RH, PAC-LH-LH and PAC-LH-RH). This direction-specific finding emerged from four tested PAC directions and should be interpreted as exploratory.

D. Associations between network metrics and clinical measures

Among the correlations between the ECDC network metrics and the FMA-UE scores (Supplementary Table S8), four reached nominal significance ($p<0.05$), all under NMES: theta GE ($\rho=+0.58$, $p=0.027$), theta LE ($\rho=+0.56$, $p=0.032$), theta K-RH ($\rho=+0.55$, $p=0.034$), and alpha-band eRMS peak amplitude ($\rho=-0.54$, $p=0.040$). None survived FDR correction for multiple comparisons. For sensory function, none of the NE metrics in the theta and alpha bands showed a significant association with the Semmes–Weinstein monofilament scores under either stimulation condition (all $p > 0.05$; FDR q = 0.869–0.949; Supplementary Table S9).

IV. Discussion

This study characterizes the immediate, modality-specific network response patterns that FVS and NMES engage in the somatosensory networks of chronic stroke survivors with unilateral lesions, within a single-session, cross-sectional design. This comparison is important for understanding the distinct roles of these two modalities in post-stroke SMI rehabilitation. Using EEG-based ECDC framework, we analyzed temporal dynamics, spectral network properties and interhemispheric functional interactions in individuals with chronic stroke and healthy controls. We found that FVS and NMES elicited distinct post-stroke somatosensory network responses, with FVS characterized by rapid theta engagement, contralesional alpha-network recruitment, and reduced interhemispheric theta–alpha coupling, whereas NMES showed stronger ipsilesional alpha-network engagement and higher interhemispheric theta–alpha coupling. The following sections elaborate on these mechanisms and their implications for SMI rehabilitation.

A. FVS promotes rapid attentional focus and ipsilesional specialization via theta network modulation

FVS confers a temporal advantage in the theta network that enables rapid attentional focus in stroke survivors, addressing post-stroke sensory processing delays. Our eRMS peak analyses show that FVS elicited a global theta network reconfiguration with significantly shorter eRMS peak latency than NMES in stroke participants (Fig. 2E). Restoring effective SMI after stroke is fundamentally limited by delayed sensory processing, a deficit closely linked to post-stroke sensory gating impairment [36]. Specifically, post-stroke demyelination and synaptic inefficiency slow the sensory gating mechanisms needed to update motor plans, hindering the brain's ability to quickly target the affected limb and initiate functional somatosensory-motor integration [37], [38]. At the electrophysiological level, the theta rhythm serves as a neural marker of involuntary attentional capture and sensory gating for novel stimuli [26], mediating the activation of the attention focus loop that constitutes the first critical step in somatosensory processing. This shortened theta latency allows FVS to potentially overcome stroke-related delays in sensory

filtering and attention, enabling the post-stroke brain to rapidly lock onto the functionally relevant limb and lay the groundwork for subsequent somatosensory coordination and SMI [40].

The spatial organization of the theta network under FVS further reinforces attentional focus and promotes ipsilesional specialization in stroke participants. Compared to NMES, FVS reduced pathologically elevated theta LE (Fig. 3B) in stroke participants toward control levels, increased ipsilesional intra-hemispheric connection density (K-RH, Fig. 3C), decreased ipsilesional connection diversity (NE-RH, Fig. 3F) and induced greater theta band lateralization toward the ipsilesional hemisphere (BAI, Fig. 3E). Compared to healthy controls, stroke participants exhibited pathologically elevated global-scale theta LE, which marks inefficient, segregated local coupling that impairs attentional focus [40]. Notably, theta LE remained higher under NMES, whereas FVS reduced theta LE toward control levels, indicating distinct modulation of sensory-gating-related theta-network organization by the two modalities. This flexible global state promotes ipsilesional specialization of the theta network, as increased K-RH and decreased NE-RH indicate concentrated but rigid network resources dedicated to localizing and processing vibratory input at the affected limb [41]. This specialization relies on the preserved dorsal column-medial lemniscus tract, a key somatosensory projection pathway [42], and theta band BAI results confirm FVS-induced lateralization toward the ipsilesional hemisphere ensures high-fidelity transmission of mechanoreceptor inputs to the contralateral S1 and reinforces targeted attentional focus [20], [23].

B. FVS facilitates alpha network resource recruitment and contralesional engagement

FVS promotes alpha network resource recruitment, laying the foundation for high-order somatosensory processing after initial attentional capture. In stroke participants, FVS induced a significantly stronger alpha-band eRMS peak amplitude than NMES (Fig. 2D), and this enhanced resource recruitment translated to whole-brain alpha network optimization with significantly increased GE and LE (Fig. 4A and B). The alpha-band eRMS peaks detected in this study signify moments of heightened, organized information integration in response to external stimuli [25]. This organized integration is critical for SMI as it guarantees the necessary cortical resource supply to support the complex neural processes involved. The optimization of GE and LE further reinforces the network's ability to efficiently transmit and process somatosensory information, building on the initial attentional focus induced by theta network regulation to facilitate high-order somatosensory processing stages [43].

FVS-induced alpha network optimization promotes contralesional engagement, helping compensate disrupted hemispheric balance in stroke participants. Somatosensory processing is collaboratively accomplished by bilateral hemispheres in healthy individuals [19], and our control group data corroborated this with balanced hemispheric involvement (BAI $\approx$ 0). In stroke participants, even as their somatosensory processing remains pathologically biased toward the ipsilesional hemisphere (BAI, Fig. 4E) under both stimulations, FVS significantly increased connection density in the contralesional hemisphere (K-LH, Fig. 4C) and normalized entropy (NE-LH, Fig. 4F) compared to NMES. High K-LH and NE-LH during FVS indicate a versatile repertoire of connections concentrated in the contralesional hemisphere [36], which enables it to handle the high computational load of somatosensory processing efficiently. By engaging this contralesional somatosensory network, FVS elicits functionally better-preserved versatile resources to guide post-stroke somatosensory processing and tends to compensate for the disrupted hemispheric balance. In contrast, NMES exerted its primary effect on the ipsilesional hemisphere. It significantly increased connection density (K-RH, Fig. 4C) and normalized entropy (NE-RH, Fig. 4F) compared to FVS, even exceeding levels seen in the control group. This finding suggests NMES strongly drives the ipsilesional alpha network. Such driving may promote network reconstruction within the lesioned regions themselves, though it may incur higher neural efficiency cost.

Because the FVS responses observed in the present study are characterized by rapid theta-band engagement and contralesional alpha-band resource recruitment, vibration intensities are expected to modulate these network responses. As FVS acts primarily on muscle mechanoreceptors, with vibration deforming muscle spindles and activating Ia afferents [11], higher intensity within the sensory range would strengthen this afferent drive, and vibration parameters such as amplitude and frequency are known to modulate the resulting neuromuscular and cortical responses [20], so these responses may amplify the magnitude of the theta and contralesional alpha responses.

C. Interhemispheric functional decoupling mediates FVS-enhanced post-stroke somatosensory processing

Interhemispheric cross-frequency functional decoupling, characterized by reduced theta–alpha PAC, is the key mechanism through which FVS co-ordinately regulates the attention focus and contralesional somatosensory engagement loops to enhance post-stroke somatosensory processing. Our PAC analyses show that, compared to NMES, FVS significantly reduced interhemispheric PAC between the ipsilesional hemisphere's theta phase and the contralesional hemisphere's alpha amplitude (PAC-RH-LH, Fig. 5D). This FVS-induced decoupling was unique to stroke participants, as it was absent in controls. Although exploratory, its coherence with the theta latency and alpha network findings across complementary analytical streams argues against it being spurious.

After stroke, maintained high PAC signifies maladaptive, constrained interhemispheric functional communication [31], [38], which is detrimental to recovery. The theta network is dysfunctional after stroke, exhibiting elevated LE and reduced connection density relative to controls (Fig. 3B–C). NMES maintained high PAC, allowing pathological theta signals from the ipsilesional hemisphere to disrupt the functional, alpha-

based somatosensory processing preserved in the contralesional hemisphere [44]. In contrast, FVS lowered PAC, promoting flexible and independent network operations [31], [38]. By reducing the cross-frequency coupling, FVS relieves theta interference and protects the contralesional alpha loop. It enables the contralesional hemisphere to fully utilize its robust connectivity (Fig. 4C, F) to compensate for the ipsilesional deficit and drive efficient somatosensory processing. In summary, FVS-induced cross-frequency decoupling acts as a critical bridge between the attention focus and contralesional engagement loops, enabling their sequential activation and forming an efficient regulatory chain that enhances post-stroke somatosensory processing.

D. Insights into the application of SMI stroke rehabilitation

These findings position FVS as a neural 'pre-conditioner' that rapidly captures attention and engages contralesional networks, addressing the somatosensory processing impairments that hinder interactive rehabilitation. Such interactive therapies, including VR- and robot-assisted training [9], [45], [46], require fast attentional focus on target muscles and efficient somatosensory processing [47], and FVS-induced contralesional engagement also mobilizes the cognitive reserve of the contralesional hemisphere to handle the cognitive load of these tasks [48]. Integrating FVS into closed-loop systems is therefore expected to provide a real-time neuromodulator of the somatosensory network.

E. Limitations and future work

Several limitations should be acknowledged. First, the single-session design and small sample size limit the assessment of longer-term network dynamics and the robustness of the observed associations with the FMA-UE and Semmes–Weinstein scores. Second, the generalizability of the findings is constrained by cohort characteristics, including the restriction to chronic stroke, the age imbalance between the control and stroke groups (67 ± 3 vs. 53 ± 11 years), and the lack of structural characterization of lesion location and size. Third, the present ECDC analysis examined only a single FVS intensity (1.9 G), precluding characterization of the intensity–response relationship.

Given these limitations, future studies should validate the identified network metrics in larger, longitudinal cohorts spanning different recovery stages and sensory impairment severities, and incorporate structural imaging to examine lesion-related variability and their predictive value for clinical recovery. Parametric studies spanning the sensory-level FVS intensity range, with vibration frequency, contact force, and individual sensory thresholds controlled, are also needed to characterize the intensity–response relationship and identify the optimal sensory vibration strength. Beyond biological and parameter validation, future work should evaluate the individual-level discriminative utility of ECDC features relative to conventional node-centric connectivity building on recently advanced deep-learning-based approaches for EEG signal and time-series classification [49], [50], and assess the reliability of the core ECDC metrics under reduced electrode montages to support low-density, portable EEG applications. Longitudinal studies combining FVS with conventional or robot-assisted rehabilitation will further be needed to determine whether the immediate network responses observed here can be maintained or consolidated and whether they relate to long-term clinical outcomes.

V. Conclusion

This study helps address an important gap in understanding the immediate cortical network effects of different somatosensory stimulations in chronic stroke by comparing FVS with sensory-level NMES using an EEG-based ECDC framework. Within our cohort, FVS was associated with a distinct network response pattern, including shorter theta-network latency, increased contralesional alpha-network diversity, and reduced theta-alpha phase-amplitude coupling between attention- and engagement-related networks. These findings highlight modality-specific network effects of FVS that may be relevant to cortical preconditioning in SMI rehabilitation. Importantly, beyond mechanistic comparison, the proposed ECDC pipeline provides an interpretable informatics approach for quantifying stimulation-related dynamic network signatures from EEG. While further validation in larger and longitudinal cohorts is needed, these network signatures may serve as candidate biomarkers for stratifying stimulation response and informing individualized neuromodulation planning in post-stroke rehabilitation.

References

[1] S. S. Kessner, U. Bingel, and G. Thomalla, "Somatosensory deficits after stroke: a scoping review," *Top. Stroke Rehabil.*, vol. 23, no. 2, pp. 136–146, Jan. 2016, doi: 10.1080/10749357.2015.1116822.

[2] L. L. Edwards, E. M. King, C. M. Buetefisch, and M. R. Borich, "Putting the 'Sensory' Into Sensorimotor Control: The Role of Sensorimotor Integration in Goal-Directed Hand Movements After Stroke," *Front. Integr. Neurosci.*, vol. 13, May 2019, doi: 10.3389/fnint.2019.00016.

[3] A. S. Asan, J. R. McIntosh, and J. B. Carmel, "Targeting Sensory and Motor Integration for Recovery of Movement After CNS Injury," *Front. Neurosci.*, vol. 15, Jan. 2022, doi: 10.3389/fnins.2021.791824.

[4] A. E. Papale and B. M. Hooks, "Circuit Changes in Motor Cortex During Motor Skill Learning," *Neuroscience*, vol. 368, pp. 283–297, Jan. 2018, doi: 10.1016/j.neuroscience.2017.09.010.

[5] Z. Guo *et al.*, "Altered Corticomuscular Coherence (CMCoh) Pattern in the Upper Limb During Finger Movements After Stroke," *Front. Neurol.*, vol. 11, p. 410, 2020, doi: 10.3389/fneur.2020.00410.

[6] S. Zhou *et al.*, "Pathway-specific cortico-muscular coherence in proximal-to-distal compensation during fine motor control of finger extension after stroke," *J. Neural Eng.*, vol. 18, no. 5, p. 056034, 2021, doi: 10.1088/1741-2552/ac20bc.

[7] L. Lin *et al.*, "Somatosensory integration in robot-assisted motor restoration post-stroke," *Front. Aging Neurosci.*, vol. 16, Nov. 2024, doi: 10.3389/fnagi.2024.1491678.

[8] X. Hu, K. Tong, V. S. Tsang, and R. Song, "Joint-angle-dependent neuromuscular dysfunctions at the wrist in persons after stroke," *Arch. Phys. Med. Rehabil.*, vol. 87, no. 5, pp. 671–679, 2006, doi: 10.1016/j.apmr.2006.02.003.

[9] L. Lin *et al.*, "Sensorimotor Integration by Targeted Priming in Muscles with Electromyography-Driven Electro-vibro-feedback in Robot-Assisted Wrist/Hand Rehabilitation after Stroke," *Cyborg Bionic Syst.*, vol. 7, p. 0507, 2026, doi: 10.34133/cbsystems.0507.

[10] M. E. Stoykov, C. Heidle, S. Kang, L. Lodesky, L. E. Maccary, and S. Madhavan, "Sensory-Based Priming for Upper Extremity Hemiparesis After Stroke: A Scoping Review," *OTJR: Occupational Therapy Journal*

of Research, vol. 42, no. 1, pp. 65–78, Jul. 2021, doi: 10.1177/15394492211032606.

[11] R. S. Calabrò *et al.*, "Is two better than one? Muscle vibration plus robotic rehabilitation to improve upper limb spasticity and function: A pilot randomized controlled trial," *PLOS One*, vol. 12, no. 10, p. e0185936, Oct. 2017, doi: 10.1371/journal.pone.0185936.

[12] C. Nam *et al.*, "An Exoneuromusculoskeleton for Self-Help Upper Limb Rehabilitation After Stroke," *Soft Rob.*, vol. 9, no. 1, pp. 14–35, 2020, doi: 10.1089/soro.2020.0090.

[13] T. Paillard, "Neuromuscular or Sensory Electrical Stimulation for Reconditioning Motor Output and Postural Balance in Older Subjects?," *Front. Physiol.*, vol. 12, Jan. 2022, doi: 10.3389/fphys.2021.779249.

[14] A. Biasiucci *et al.*, "Brain-actuated functional electrical stimulation elicits lasting arm motor recovery after stroke," *Nat. Commun.*, vol. 9, no. 1, Jun. 2018, doi: 10.1038/s41467-018-04673-z.

[15]L. Lin *et al.*, "Mobile Upper Limb Robots for Self-Help Telerehabilitation," in *Automation in Tele-Neurorehabilitation*, Boca Raton: CRC Press, 2025, pp. 94–107. doi: 10.1201/9781003419235-6.

[16] Y. Huang *et al.*, "A comparison of the rehabilitation effectiveness of neuromuscular electrical stimulation robotic hand training and pure robotic hand training after stroke: A randomized controlled trial," *Biomed. Signal Process. Control*, vol. 56, p. 101723, 2020, doi: 10.1016/j.bspc.2019.101723.

[17] P. Hautasaari, U. M. Kujala, and I. M. Tarkka, "Detecting differences with magnetoencephalography of somatosensory processing after tactile and electrical stimuli," *J. Neurosci. Methods*, vol. 311, pp. 331–337, Jan. 2019, doi: 10.1016/j.jneumeth.2018.09.014.

[18] A. Insausti-Delgado, E. López-Larraz, J. Omedes, and A. Ramos-Murguialday, "Intensity and Dose of Neuromuscular Electrical Stimulation Influence Sensorimotor Cortical Excitability," *Front. Neurosci.*, vol. 14, Jan. 2021, doi: 10.3389/fnins.2020.593360.

[19] L. Lin *et al.*, "Comparison of Immediate Neuromodulatory Effects between Focal Vibratory and Electrical Sensory Stimulations after Stroke," *Bioengineering*, vol. 11, no. 3, p. 286, 2024, doi: 10.3390/bioengineering11030286.

[20] R. Souron, T. Besson, G. Y. Millet, and T. Lapole, "Acute and chronic neuromuscular adaptations to local vibration training," *Eur. J. Appl. Physiol.*, vol. 117, no. 10, pp. 1939–1964, Aug. 2017, doi: 10.1007/s00421-017-3688-8.

[21] A. Jackson and J. B. Zimmermann, "Neural interfaces for the brain and spinal cord—restoring motor function," *Nat. Rev. Neurol.*, vol. 8, no. 12, pp. 690–699, Nov. 2012, doi: 10.1038/nrneurol.2012.219.

[22] J. Wu *et al.*, "Connectivity measures are robust biomarkers of cortical function and plasticity after stroke," *Brain*, vol. 138, no. 8, pp. 2359–2369, Jun. 2015, doi: 10.1093/brain/awv156.

[23] W. Li, C. Li, Q. Xu, and L. Ji, "Effects of Focal Vibration over Upper Limb Muscles on the Activation of Sensorimotor Cortex Network: An EEG Study," *J. Healthcare Eng.*, vol. 2019, pp. 1–7, May 2019, doi: 10.1155/2019/9167028.

[24] J. Faskowitz, F. Z. Esfahlani, Y. Jo, O. Sporns, and R. F. Betzel, "Edge-centric functional network representations of human cerebral cortex reveal overlapping system-level architecture," *Nat. Neurosci.*, vol. 23, no. 12, pp. 1644–1654, Oct. 2020, doi: 10.1038/s41593-020-00719-y.

[25] R. F. Betzel, J. Faskowitz, and O. Sporns, "Living on the edge: network neuroscience beyond nodes," *Trends Cognit. Sci.*, vol. 27, no. 11, pp. 1068–1084, Nov. 2023, doi: 10.1016/j.tics.2023.08.009.

[26] F. Zamani Esfahlani *et al.*, "High-amplitude cofluctuations in cortical activity drive functional connectivity," *Proceedings of the National Academy of Sciences*, vol. 117, no. 45, pp. 28393–28401, Oct. 2020, doi: 10.1073/pnas.2005531117.

[27] J. Li, D. Feng, G. Xu, and J. Song, "Hierarchical Features of Brain EEG Edge-Centric Networks Predict Mild Brain Injury," in *2025 44th Chinese Control Conference (CCC)*, Chongqing, China: IEEE, Jul. 2025, pp. 980–984. doi: 10.23919/ccc64809.2025.11179253.

[28] P. Sorrentino *et al.*, "Dynamical interactions reconfigure the gradient of cortical timescales," *Network Neurosci.*, vol. 7, no. 1, pp. 73–85, Jan. 2023, doi: 10.1162/netn_a_00270.

[29] L. Pion-Tonachini, K. Kreutz-Delgado, and S. Makeig, "ICLabel: An automated electroencephalographic independent component classifier, dataset, and website," *Neuroimage*, vol. 198, pp. 181–197, Sep. 2019, doi: 10.1016/j.neuroimage.2019.05.026.

[30] A. K. Engel, C. Gerloff, C. C. Hilgetag, and G. Nolte, "Intrinsic Coupling Modes: Multiscale Interactions in Ongoing Brain Activity," *Neuron*, vol. 80, no. 4, pp. 867–886, Nov. 2013, doi: 10.1016/j.neuron.2013.09.038.

[31] A. S. Keller, L. Payne, and R. Sekuler, "Characterizing the roles of alpha and theta oscillations in multisensory attention," *Neuropsychologia*, vol. 99, pp. 48–63, May 2017, doi: 10.1016/j.neuropsychologia.2017.02.021.

[32] S. Lopez *et al.*, "Electroencephalographic sensorimotor rhythms are modulated in the acute phase following focal vibration in healthy subjects," *Neuroscience*, vol. 352, pp. 236–248, Jun. 2017, doi: 10.1016/j.neuroscience.2017.03.015.

[33] J.-P. Lachaux, E. Rodriguez, J. Martinerie, and F. J. Varela, "Measuring phase synchrony in brain signals," *Hum. Brain Mapp.*, vol. 8, no. 4, pp. 194–208, 1999, doi: 10.1002/(SICI)1097-0193(1999)8:4<194::AID-HBM4>3.0.CO;2-C.

[34] S. Zhou *et al.*, "Impairments of cortico-cortical connectivity in fine tactile sensation after stroke," *J. NeuroEng. Rehabil.*, vol. 18, no. 1, p. 34, 2021, doi: 10.1186/s12984-021-00821-7.

[35] M. Rubinov and O. Sporns, "Complex network measures of brain connectivity: Uses and interpretations," *Neuroimage*, vol. 52, no. 3, pp. 1059–1069, Sep. 2010, doi: 10.1016/j.neuroimage.2009.10.003.

[36] Y. Jo, F. Zamani Esfahlani, J. Faskowitz, E. J. Chumin, O. Sporns, and R. F. Betzel, "The diversity and multiplexity of edge communities within and between brain systems," *Cell Rep.*, vol. 37, no. 7, p. 110032, Nov. 2021, doi: 10.1016/j.celrep.2021.110032.

[37] R. A. Seymour, G. Rippon, and K. Kessler, "The Detection of Phase Amplitude Coupling during Sensory Processing," *Front. Neurosci.*, vol. 11, Sep. 2017, doi: 10.3389/fnins.2017.00487.

[38] A. B. L. Tort, R. Komorowski, H. Eichenbaum, and N. Kopell, "Measuring Phase-Amplitude Coupling Between Neuronal Oscillations of Different Frequencies," *J. Neurophysiol.*, vol. 104, no. 2, pp. 1195–1210, Aug. 2010, doi: 10.1152/jn.00106.2010.

[39] E. Maris and R. Oostenveld, "Nonparametric statistical testing of EEG- and MEG-data," *J. Neurosci. Methods*, vol. 164, no. 1, pp. 177–190, Aug. 2007, doi: 10.1016/j.jneumeth.2007.03.024.

[40] A. K. Bonkhoff *et al.*, "Abnormal dynamic functional connectivity is linked to recovery after acute ischemic stroke," *Hum. Brain Mapp.*, vol. 42, no. 7, pp. 2278–2291, Mar. 2021, doi: 10.1002/hbm.25366.

[41] J. N. Williamson *et al.*, "Cortical Reorganization of Early Somatosensory Processing in Hemiparetic Stroke," *Journal of Clinical Medicine*, vol. 11, no. 21, p. 6449, Oct. 2022, doi: 10.3390/jcm11216449.

[42] U. Proske and S. C. Gandevia, "The Proprioceptive Senses: Their Roles in Signaling Body Shape, Body Position and Movement, and Muscle Force," *Physiol. Rev.*, vol. 92, no. 4, pp. 1651–1697, Oct. 2012, doi: 10.1152/physrev.00048.2011.

[43] T. R. Ruikes, J. Fiorilli, J. Lim, G. Huis in 't Veld, C. Bosman, and C. M. A. Pennartz, "Theta Phase Entrainment of Single-Cell Spiking in Rat Somatosensory Barrel Cortex and Secondary Visual Cortex Is Enhanced during Multisensory Discrimination Behavior," *eneuro*, vol. 11, no. 4, p. ENEURO.0180-23.2024, Apr. 2024, doi: 10.1523/ENEURO.0180-23.2024.

[44] S. C.-J. Chen, M.-J. Hsu, Y.-T. Kuo, R.-T. Lin, S.-K. Lo, and J.-H. Lin, "Immediate effects of noxious and innocuous thermal stimulation on brain activation in patients with stroke," *Medicine (Baltimore)*, vol. 99, no. 9, p. e19386, Feb. 2020, doi: 10.1097/md.0000000000019386.

[45] Y. Huang, W. P. Lai, Q. Qian, X. Hu, E. W. C. Tam, and Y. Zheng, "Translation of robot-assisted rehabilitation to clinical service: a comparison of the rehabilitation effectiveness of EMG-driven robot hand assisted upper limb training in practical clinical service and in clinical trial with laboratory configuration for chronic stroke," *Biomed. Eng. Online*, vol. 17, no. 1, p. 91, 2018, doi: 10.1186/s12938-018-0516-2.

[46] K. E. Laver *et al.*, "Virtual reality for stroke rehabilitation," *Cochrane Db. Syst. Rev.*, vol. 2025, no. 6, Jun. 2025, doi: 10.1002/14651858.CD008349.pub5.

[47] R. Gassert and V. Dietz, "Rehabilitation robots for the treatment of sensorimotor deficits: a neurophysiological perspective," *J. NeuroEng. Rehabil.*, vol. 15, no. 1, Jun. 2018, doi: 10.1186/s12984-018-0383-x.

[48] W. Klimesch, "Alpha-band oscillations, attention, and controlled access to stored information," *Trends Cognit. Sci.*, vol. 16, no. 12, pp. 606–617, Dec. 2012, doi: 10.1016/j.tics.2012.10.007.

[49] Z. Xiao and Q. Wan, "Feature-Enriched Mutual Distillation with Semi-Supervised Contrastive Learning for Electroencephalogram Signal Classification," *ACM Trans. Comput. Healthcare*, vol. 7, no. 2, pp. 1–26, Apr. 2026, doi: 10.1145/3798094.

[50] Z. Xiao, Q. Wan, W. Ding, F. Song, and H. Tong, "Knowledge Aware State-Space Capsule Network for Multivariate Time Series Classification," *IEEE Trans. Knowl. Data Eng.*, vol. 38, no. 8, pp. 5215–5231, Aug. 2026, doi: 10.1109/TKDE.2026.3692700.

Supplementary material

Participants

Participants after stroke were screened and recruited from local districts. The inclusion criteria were as follows: (i) at least 6 months after the onset of a unilateral lesion in the cortical or subcortical regions due to stroke [1]; (ii) sufficient cognition to follow experimental instructions (Mini-Mental State Examination (MMSE) score > 23 [2]); (iii) moderate-to-severe motor disability in the affected upper limb (15 < Fugl–Meyer assessment (FMA) < 45) [3, 4]; (iv) muscle spasticity scores ≤ 3 at the wrist and fingers, as measured by the modified Ashworth scale (MAS) [5]; (v) a normal-to-diminished protective sensation on the affected forearm under a threshold of 4.31 (2.0 g) as measured by the Semmes-Weinstein monofilament test [6, 7] on the skin surface above the muscle union of the flexor carpi radialis(FCR) and flexor digitorum (FD) (i.e. FCR-FD) and the muscle union of the extensor carpi ulnaris (ECU) and extensor digitorum (ED) (i.e. ECU-ED) of the paretic forearm; (vi) no neurological impairments except for stroke; and (vii) right-handed before the stroke onset. The exclusion criteria for stroke participants were (i) post-stroke pain; (ii) epilepsy; (iii) cerebral implantation; and (iv) pacemaker implantation. Unimpaired participants were also recruited from the local districts; their inclusion criteria were right-handed and there was no history of neurological, psychiatric, cardiovascular, cognitive, or mental impairments. The clinical assessments mentioned above were carried out by an independent assessor who was blinded to the content of the study. Finally, fifteen stroke participants (i.e. the stroke group) and fifteen unimpaired participants (i.e. the control group) were recruited. All participants understood the study's research information and signed the consent form before the experiment. Supplementary Table S1 provides an overview of the demographic information of all the individuals involved in the study. The clinical scores of the stroke participants are presented in Supplementary Table S2.

Experiment setup and protocol

The participant was requested to take a comfortable seated position facing a table, with an eye mask and a pair of earplugs to further minimize visual and auditory interference during the EEG recording. Then, they were instructed to reach their testing forearm forward, with

the elbow resting at approximately 170◦ and supported by a cushion. The wrist and finger joints remained in a relaxed position. The contralateral upper limb was positioned naturally on the participant's thigh. A 64-channel EEG cap was mounted on the scalp of the participant according to the standard 10-10 system (Fig. 1A) [8].

To enhance motor unit recruitment, the NMES electrode pairs were placed in the common area of the motor points for muscle bellies of the FCR-FD or ECU-ED muscle union [9, 10]. A miniature FVS vibration motor was gently pressed against the participant's skin using medical tape between the cathode and anode of the NMES electrodes to ensure vibration transmission [11].

Based on the above setup, eight FVS and NMES schemes with different intensities were applied over the FCR-FD or ECU-ED muscle union. The FVS schemes had five intensities from 0.7 G to 1.9 G below the threshold of the tonic vibration reflex without involuntary muscle contraction, i.e. all FVS intensities were at sensory level. The NMES schemes had three intensities: (1) the motor threshold (NMES-1), identified as the initial twitching of the fingers; (2) the representative sensory-level NMES (NMES-2), calculated as the median value between the perceptual and motor thresholds; and (3) the perceptual threshold (NMES-3), identified as the initial tingling sensation on the forearm. All these intensities were reported for sensory rehabilitation post-stroke [12, 13] and could be effectively perceived and tolerable for the sustained stimulation of human participants [14]. There were eight trials associated with the eight stimulation schemes applied to a muscle union in random order, forming the stimulation protocol. Each trial included six repeated stimulation blocks of the same stimulation scheme. See ref [15] for details on the experiment protocol.

Supplementary Table S1 Demographic data of the participants

Group	NO. of participants	Stroke Type (Hemorrhage /Ischemic)	Affected Arm (Left/Right)	Gender (Male/Female)	Age (Years, Mean ± SD)	Years after Stroke (Min/Max Years)
Stroke	15	9/6	10/5	8/7	53±11	2/18
Control	15	-/-	-/-	9/6	67±3	-/-

Supplementary Table S2 Clinical scores of the stroke participants

Clinical assessment	FMA	MAS		Monofilament			
	Upper extremity	Wrist	Finger	Affected Extensor	Affected Flexor	Unaffected Extensor	Unaffected Flexor
Score (mean±SD)	31.1±11.5	1.1±0.9	1.9±0.8	3.23±0.67	3.24±0.49	3±0.45	3.26±0.38

Supplementary Table S3 Node-centric and edge-centric measures

<table>
<tr><td colspan="2">Basic concepts and notation</td><td colspan="2">N is the set of all nodes in the network, and n is the number of nodes.
N_{LH} and N_{RH} is the ser of all nodes in the left and right hemisphere, respectively. $N_s = N_{LH}|N_{RH}$.
a_{ij} is the connection status between i and j: $a_{ij} = 1$ where edge (i, j) exists (when i and j are neighbours); $a_{ij} = 0$ otherwise ($a_{ii} = 0$ for all i).
The number of edges as $l = \sum_{i,j \in N} a_{ij}$.</td></tr>
<tr><td></td><td>Scale</td><td>Measures</td><td>Formula</td></tr>
<tr><td rowspan="8">Node-centric</td><td>Temporal</td><td>eRMS</td><td>$eRMS(t) = R_{block}(t) - \overline{R_{baseline}(t)}$

$R(t) = \sqrt{\frac{1}{M}\sum_{i,j,i\neq j} eTS_{i,j}(t)^2}$

where $R_{block}(t)$ was the RMS waveform during the stimulation period and $\overline{R_{baseline}(t)}$ was the mean value over the baseline period in the eTS matrices (Fig.1B). M represented the number of unique channel pairs (edges).</td></tr>
<tr><td rowspan="3">Large</td><td>Global efficiency (GE) [16]</td><td>$GE = \frac{1}{n}\sum_{i \in N} E_i = \frac{1}{n}\sum_{i \in N} \frac{\sum_{j\in N, j\neq i} d_{ij}^{-1}}{n-1}$,

where i and j are nodes of interest ($i, j \in$ N), E_i is the efficiency of node i and all other nodes and d_{ij} is length of the shortest path between nodes i and j.</td></tr>
<tr><td>Local efficiency (LE) [16]</td><td>$LE = \frac{1}{n}\sum_{i \in N} E_{loc,i} = \frac{1}{n}\sum_{i \in N} \frac{\sum_{j,h\in N, j\neq i} a_{ij}a_{ih}[d_{jh}(N_i)]^{-1}}{k_i(k_i-1)}$,

where $E_{loc,i}$ is the local efficiency of node i, and $d_{jh}(N_i)$ is the length of the shortest path between j and h, that contains only neighbours of i.</td></tr>
<tr><td colspan="2">GE are typically used to evaluate the ability to rapidly combine specialized information from distributed brain regions. LE illustrates the brain network efficiency of processing information in partial regions (functional segregation), evaluating the resistance of brain networks to small-scale malfunction.</td></tr>
<tr><td rowspan="3">Intermediate</td><td>Inter-density (K-inter) [17, 18]</td><td>$K\text{-}inter = \frac{1}{N_s^2}\sum_{i \in N_{LH}, j \in N_{RH}} a_{ij}$</td></tr>
<tr><td>Intra-density (K-intra) [17, 18]</td><td>$K\text{-}intra = \frac{2}{N_s^2 - N_s}\sum_{i \neq j \in N_s} a_{ij}$</td></tr>
<tr><td colspan="2">The intra- and inter-group differences of density K between and within the hemispheres reflect the compensation and lateralization in the alteration of brain connectivity post-stroke.</td></tr>
<tr><td rowspan="3">Small</td><td>Node strength (NS) [19]</td><td>$NS = l = \sum_{i,j \in N} a_{ij}$.</td></tr>
<tr><td>Brain asymmetry index (BAI) [20]</td><td>$BAI = \frac{1}{N_{RH}}\sum_{i=1}^{N_{RH}} NS_i - \frac{1}{N_{LH}}\sum_{j=1}^{N_{LH}} NS_j$</td></tr>
<tr><td colspan="2">NS and BAI measure the involvement and laterality of local brain areas, respectively.</td></tr>
<tr><td>Edge-centric</td><td>Intermediate</td><td>Normalized entropy for inter-</td><td>$NE\text{-}intra_i = -\sum_c p_{ic}\log_2 p_{ic}$</td></tr>
</table>

		hemispheric edges (NE-inter) [21, 22]	$p_{ic} = \frac{1}{N-1}\sum_{i \in N_{LH}, j \in N_{RH}} \delta(g_{ij}, c)$,
		Normalized entropy for intra-hemispheric edges (NE-intra) [21, 22]	$NE\text{-}inter_i = -\sum_c p_{ic} \log_2 p_{ic}$ $p_{ic} = \frac{1}{N-1}\sum_{i \in i \neq j \in N_s} \delta(g_{ij}, c)$,
		where $g_{ij} \in \{1,\ldots,k\}$ was the cluster assignment of the edge linking node *i* and *j*, and $\delta(x, y)$ is the Kronecker delta, whose value is 1 if *x*=*y* and 0 otherwise. $\sum_x p_{ic} = 1$, the vector $p_i = [p_{i1}, \ldots, p_{ik}]$ was a probability distribution	

Supplementary Table S4 Statistics results of the amplitude and latency of eRMS peaks across frequency bands.

			Stroke	**Control**	**Inter-group Diff.**
Bands	**Peak**	**Stimulation**	**Mean ± SE**		***P* (EFs)**
Theta	Amplitude	FVS	0.020±0.008	0.057±0.008	**0.003$^{\#\#}$ (*d* = 1.193)**
		NMES	0.027±0.006	0.025±0.009	**0.384 (*A* = 0.596)**
	Intra-group Diff. — *P* (ES)		**0.481 (*d* = 0.268)**	**0.018* (*r* = 0.683)**	-
	Latency	FVS	0.236±0.096	0.305±0.078	**0.582 (*d* = 0.203)**
		NMES	0.502±0.080	0.296±0.097	**0.112 (*d* = 0.600)**
	Intra-group Diff. — *P* (ES)		**0.045* (*d* = 0.778)**	**0.935 (*d* = 0.026)**	-
Alpha	Amplitude	FVS	0.038±0.006	0.048±0.011	**0.398 (*d* = 0.314)**
		NMES	0.021±0.006	0.042±0.009	**0.075 (*d* = 0.679)**
	Intra-group Diff. — *P* (ES)		**0.010* (*d* = 0.650)**	**0.640 (*d* = 0.168)**	-
	Latency	FVS	0.376±0.054	0.341±0.053	**0.645 (*d* = 0.170)**
		NMES	0.451±0.089	0.460±0.074	**0.756 (*A*= 0.536)**
	Intra-group Diff. — *P* (ES)		**0.489 (*r* = -0.217)**	**0.171 (*d* = 0.476)**	-

Inter-group Diff.: Inter-group difference calculated by independent *t*-test or Mann–Whitney U-test; Intra-group Diff.: Inter-group difference calculated by paired *t*-test or Wilcoxon signed-rank test. EFs: Effect size; d: Cohen's d for independent/paired *t*-test; A: Vargha and Delaney's A for Mann–Whitney U-test; r: Rank-Biserial Correlation for Wilcoxon signed-rank test.

Supplementary Table S5 Theta-band results of node-centric and edge-centric measures.

			Stroke	**Control**	**Inter-group Diff.**
Scale	**Measure**	**Stimulation**	**Mean ± SE**		***P* (EFs)**
Global	GE	FVS	0.513±0.001	0.518±0.003	**0.089 (*d* = 0.65)**
		NMES	0.513±0.003	0.514±0.004	**0.779 (*d* = 0.10)**
	Intra-group Diff. — *P* (ES)		**0.942 (*d* = 0.03)**	**0.394 (*d* = 0.33)**	-
	LE	FVS	0.153±0.006	0.119±0.004	**0.000$^{\#\#\#}$ (*d* = 1.80)**
		NMES	0.298±0.010	0.054±0.002	**0.000$^{\#\#\#}$ (*d* = 8.80)**
	Intra-group Diff. — *P* (ES)		**0.000*** (*d* = 4.60)**	**0.000*** (*d* = 5.34)**	-
Intermediate	K-inter	FVS	0.134±0.003	0.143±0.003	**0.015$^{\#}$ (*d* = 0.94)**
		NMES	0.107±0.002	0.139±0.003	**0.000$^{\#\#\#}$ (*d* = 3.54)**
	Intra-group Diff. — *p* (ES)		**0.000*** (*d* = 3.22)**	**0.190 (*d* = 0.42)**	-
	K-RH	FVS	0.111±0.003	0.123±0.003	**0.008$^{\#\#}$ (*d* = 1.05)**
		NMES	0.054±0.001	0.128±0.003	**0.000$^{\#\#\#}$ (*d* = 8.96)**
	Intra-group Diff. — P (ES)		**0.000***(*d* = 7.46)**	**0.165 (*d* = 0.44)**	-
	K-LH	FVS	0.105±0.002	0.177±0.004	**0.000$^{\#\#\#}$ (*d* = 6.69)**
		NMES	0.161±0.004	0.165±0.003	**0.467 (*d* = 0.27)**
	Intra-group Diff. — *P* (ES)		**0.000*** (*d* = 4.89)**	**0.034* (*d* = 0.87)**	-

	NE-inter	FVS	0.829±0.009	0.824±0.008	**0.292 (*A* = 0.60)**
		NMES	0.919±0.008	0.902±0.002	**0.421 (*A* = 0.58)**
	Intra-group Diff. — *P* (ES)		**0.000*** (*r* = -1.00)**	**0.000*** (*r* = -1.00)**	-
	NE-RH	FVS	0.716±0.007	0.628±0.005	**0.000$^{\#\#\#}$ (*A* = 0.98)**
		NMES	0.788±0.006	0.706±0.016	**0.000$^{\#\#\#}$ (*A* = 1.00)**
	Intra-group Diff. — *P* (ES)		**0.000*** (*r* = -1.00)**	**0.000*** (*r* = -1.00)**	-
	NE-LH	FVS	0.754±0.006	0.632±0.004	**0.000$^{\#\#\#}$ (*A* = 1.00)**
		NMES	0.488±0.034	0.549±0.006	**0.296 (*A* = 0.40)**
	Intra-group Diff. — *P* (ES)		**0.000*** (*r* = 1.00)**	**0.000*** (*r* = 1.00)**	-
Small	BAI	FVS	0.761±0.079	0.700±0.005	**0.494 (*d* = 0.25)**
		NMES	0.533±0.030	0.508±0.007	**0.690 (*d* = 0.15)**
	Intra-group Diff. — *P* (ES)		**0.014* (*d* = 0.99)**	**0.018* (*d* = 0.89)**	-

Inter-group Diff.: Inter-group difference calculated by independent *t*-test or Mann–Whitney U-test; Intra-group Diff.: Inter-group difference calculated by paired *t*-test or Wilcoxon signed-rank test. EFs: Effect size; d: Cohen's d for independent/paired *t*-test; A: Vargha and Delaney's A for Mann–Whitney U-test; r: Rank-Biserial Correlation for Wilcoxon signed-rank test.

Supplementary Table S6 Alpha-band results of node-centric and edge-centric measures.

			Stroke	**Control**	**Inter-group Diff.**
Scale	**Measure**	**Stimulation**	**Mean ± SE**		***P* (EFs)**
Global	GE	FVS	0.575±0.003	0.574±0.002	**0.868 (*A* = 0.52)**
		NMES	0.551±0.003	0.545±0.003	**0.051 (*A* = 0.71)**
	Intra-group Diff. — *P* (ES)		**0.000*** (*r* = 1.00)**	**0.000*** (*r* = 1.00)**	-
	LE	FVS	0.088±0.006	0.277±0.008	**0.000$^{\#\#\#}$ (*d* = 6.56)**
		NMES	0.068±0.003	0.094±0.005	**0.000$^{\#\#\#}$ (*d* = 1.59)**
	Intra-group Diff. — *P* (ES)		**0.004** (*d* = 1.00)**	**0.000*** (*d*= 6.85)**	-
Intermediate	K-inter	FVS	0.311±0.007	0.340±0.008	**0.015$^{\#}$ (*d* = 0.94)**
		NMES	0.296±0.007	0.312±0.010	**0.074 (*A* = 0.31)**
	Intra-group Diff. — *P* (ES)		**0.107 (*r* = 0.483)**	**0.083 (*r* = 0.52)**	-
	K-RH	FVS	0.094±0.003	0.051±0.002	**0.000$^{\#\#\#}$ (*d* = 5.12)**
		NMES	0.131±0.003	0.052±0.002	**0.000$^{\#\#\#}$ (*A* = 1.00)**
	Intra-group Diff. — *P* (ES)		**0.000*** (*d* = 3.40)**	**0.277(*r* = -0.33)**	-
	K-LH	FVS	0.030±0.001	0.098±0.002	**0.000$^{\#\#\#}$ (*d* = 9.65)**
		NMES	0.012±0.001	0.058±0.002	**0.000$^{\#\#\#}$ (*d* = 7.24)**
	Intra-group Diff. — *P* (ES)		**0.000*** (*d* = 6.15)**	**0.000*** (*d* = 4.48)**	-
	NE-inter	FVS	0.893±0.008	0.786±0.008	**0.000$^{\#\#\#}$ (*A* = 1.00)**
		NMES	0.932±0.001	0.896±0.003	**0.000$^{\#\#\#}$ (*A* = 1.00)**
	Intra-group Diff. — *P* (ES)		**0.000*** (*r* = -0.86)**	**0.000*** (*r* = -1.0)**	-
	NE-RH	FVS	0.697±0.011	0.526±0.006	**0.000$^{\#\#\#}$ (*A* = 1.00)**
		NMES	0.800±0.008	0.667±0.008	**0.000$^{\#\#\#}$ (*A* = 1.00)**
	Intra-group Diff. — *P* (ES)		**0.000*** (*r* = -0.99)**	**0.000*** (*r* = -1.0)**	-
	NE-LH	FVS	0.676±0.005	0.570±0.010	**0.000$^{\#\#\#}$ (*A* = 1.00)**
		NMES	0.493±0.020	0.567±0.012	**0.004$^{\#\#}$ (*A* = 0.24)**
	Intra-group Diff. — *P* (ES)		**0.000*** (*r* = 1.00)**	**0.812 (*r* = 0.07)**	-
Small	BAI	FVS	0.998±0.079	0.095±0.007	**0.000$^{\#\#\#}$ (*d* = 4.18)**
		NMES	0.832±0.030	0.158±0.010	**0.000$^{\#\#\#}$ (*d* = 7.75)**
	Intra-group Diff. — *P* (ES)		**0.075 (*d* = 0.72)**	**0.000*** (*d* = 1.86)**	-

Inter-group Diff.: Inter-group difference calculated by independent *t*-test or Mann–Whitney U-test; Intra-group Diff.: Inter-group difference calculated by paired *t*-test or Wilcoxon signed-rank test. EFs: Effect size; d: Cohen's d for independent/paired *t*-test; A: Vargha and Delaney's A for Mann–Whitney U-test; r: Rank-Biserial Correlation for Wilcoxon signed-rank test.

Supplementary Table S7 Statistics results of PAC.

		Stroke	Control	Inter-group Diff.
PAC	**Stimulation**	**Mean (10^{-3}) ± SE (10^{-5})**		***P* (EFs)**
LH-LH	FVS	0.917±4.78	1.014±4.38	**0.147 (*d* =0.545)**
	NMES	1.006±3.51	0.972±3.45	**0.506 (*d* =0.246)**
Intra-group Diff. — *P* (ES)		**0.106 (*d* = 0.54)**	**0.498 (*d* = 0.27)**	-
RH-RH	FVS	0.934±3.77	1.045±3.91	**0.050 (*d* = 0.747)**
	NMES	1.010±3.76	1.051±3.83	**0.458 (*d* = 0.37)**
Intra-group Diff. — *P* (ES)		**0.070 (*d* = 0.52)**	**0.893 (*d* = 0.04)**	-
LH-RH	FVS	0.972±4.13	1.039±4.62	**0.287 (*d* = 0.40)**
	NMES	1.000±3.94	1.024±4.75	**0.700(*d* =0.142)**
Intra-group Diff. — *P* (ES)		**0.506 (*d* = 0.18)**	**0.764 (*d* = 0.09)**	-
RH-LH	FVS	0.881±4.13	1.018±3.12	**0.023$^{\#}$ (*A* = 0.25)**
	NMES	0.988±4.16	0.996±2.52	**0.872 (*d* = 0.059)**
Intra-group Diff. — *P* (ES)		**0.021* (*d* = 0.67)**	**0.720 (*r* = 0.12)**	-

Inter-group Diff.: Inter-group difference calculated by independent *t*-test or Mann–Whitney U-test; Intra-group Diff.: Inter-group difference calculated by paired *t*-test or Wilcoxon signed-rank test. EFs: Effect size; d: Cohen's d for independent/paired *t*-test; A: Vargha and Delaney's A for Mann–Whitney U-test; r: Rank-Biserial Correlation for Wilcoxon signed-rank test.

Supplementary Table S8. Spearman correlations between FMA-UE and ECDC features in the stroke group (n=15).

Dimension	Metric	θ-FVSρ (p)	θ-NMESρ (p)	α-FVSρ (p)	α-NMESρ (p)
Temporal dynamics	Peak amplitude	+0.02 (0.939)	+0.19 (0.495)	−0.09 (0.748)	**−0.54 (0.040)**
	Latency	−0.23 (0.415)	−0.39 (0.141)	+0.23 (0.408)	+0.28 (0.297)
Node-centric(large-scale)	Global efficiency (GE)	+0.03 (0.925)	**+0.58 (0.027)**	+0.14 (0.626)	+0.43 (0.112)
	Local efficiency (LE)	+0.06 (0.824)	**+0.56 (0.032)**	+0.21 (0.454)	+0.01 (0.981)
Node-centric(intermediate-scale)	K-inter	+0.15 (0.584)	+0.40 (0.143)	+0.18 (0.500)	+0.44 (0.100)
	K-RH	+0.26 (0.355)	**+0.55 (0.034)**	−0.11 (0.670)	+0.03 (0.907)
	K-LH	−0.09 (0.758)	+0.34 (0.216)	+0.37 (0.172)	+0.32 (0.241)
Node-centric(small-scale)	Brain asymmetry index (BAI)	−0.28 (0.306)	+0.22 (0.420)	−0.07 (0.809)	+0.05 (0.860)
Edge-centric	NE-inter	+0.25 (0.373)	+0.30 (0.287)	+0.24 (0.390)	−0.20 (0.467)
	NE-RH	−0.05 (0.862)	−0.26 (0.347)	−0.12 (0.672)	−0.15 (0.584)
	NE-LH	+0.27 (0.319)	+0.18 (0.523)	+0.23 (0.406)	+0.10 (0.729)

Note: ρ = Spearman rank correlation coefficient, p = permutation-based p-value (10,000 permutations). Bold values indicate nominal significance (p < 0.05). FDR correction across the 44 tested correlations (Benjamini–Hochberg) yielded a q of 0.441 for all four nominally significant correlations, none of which survived the correction.

Supplementary Table S9. Spearman correlations between Semmes-Weinstein monofilament scores (affected side) and normalized entropy (NE) metrics in the stroke group (n=15).

NE metric	θ-FVSρ (p)	θ-NMESρ (p)	α-FVSρ (p)	α-NMESρ (p)
NE-RH	−0.10 (0.731)	+0.22 (0.444)	+0.44 (0.099)	−0.18 (0.512)
NE-LH	−0.39 (0.156)	+0.07 (0.797)	+0.02 (0.949)	−0.15 (0.580)
NE-inter	+0.14 (0.620)	+0.08 (0.786)	+0.24 (0.393)	+0.18 (0.518)

Note: ρ = Spearman rank correlation coefficient, p = permutation-based p-value (10,000 permutations). None of the twelve correlations reached significance (all p > 0.05, FDR q ranged from 0.869 to 0.949).

References in supplementary material

[1] X. Hu, K. Tong, V. S. Tsang, and R. Song, "Joint-angle-dependent neuromuscular dysfunctions at the wrist in persons after stroke," *Arch. Phys. Med. Rehabil.*, vol. 87, no. 5, pp. 671–679, 2006, doi: 10.1016/j.apmr.2006.02.003.

[2] T. N. Tombaugh and N. J. McIntyre, "The mini-mental state examination: a comprehensive review," *J. Am. Geriatr. Soc.*, vol. 40, no. 9, pp. 922–935, 1992, doi: 10.1111/j.1532-5415.1992.tb01992.x.

[3] K. J. Sullivan *et al.,* "Fugl-Meyer assessment of sensorimotor function after stroke: standardized training procedure for clinical practice and clinical trials," *Stroke*, vol. 42, no. 2, pp. 427–432, 2011, doi: 10.1161/STROKEAHA.110.592766.

[4] C. Nam *et al.,* "Home-based self-help telerehabilitation of the upper limb assisted by an electromyography-driven wrist/hand exoneuromusculoskeleton after stroke," *J. NeuroEng. Rehabil.*, vol. 18, no. 1, p. 137, 2021, doi: 10.1186/s12984-021-00930-3.

[5] R. W. Bohannon and M. B. Smith, "Interrater reliability of a modified Ashworth scale of muscle spasticity," *Phys. Ther.*, vol. 67, no. 2, pp. 206–207, 1987, doi: 10.1093/ptj/67.2.206.

[6] M. Suda *et al.,* "Validity and Reliability of the Semmes-Weinstein Monofilament Test and the Thumb Localizing Test in Patients With Stroke," *Front. Neurol.*, vol. 11, p. 625917, 2020, doi: 10.3389/fneur.2020.625917.

[7] S. M. Perle, M. J. Schneider, and D. R. Seaman, "Chiropractic Management of Peripheral Neuropathy: Pathophysiology, Assessment, and Treatment," *Top. Clin. Chiropr.*, 1999.

[8] M. Seeck *et al.,* "The standardized EEG electrode array of the IFCN," *Clin. Neurophysiol.*, vol. 128, no. 10, pp. 2070–2077, 2017, doi: 10.1016/j.clinph.2017.06.254.

[9] C. Nam *et al.,* "An Exoneuromusculoskeleton for Self-Help Upper Limb Rehabilitation After Stroke," *Soft Robot.*, 2020, doi: 10.1089/soro.2020.0090.

[10] Y. Muraoka, "Development of an EMG recording device from stimulation electrodes for functional electrical stimulation," *Front Med. Biol. Eng.*, vol. 11, no. 4, pp. 323–333, 2002, doi: 10.1163/156855701321138969.

[11] S. Choi and K. J. Kuchenbecker, "Vibrotactile Display: Perception, Technology, and Applications," *Proc. IEEE*, vol. 101, no. 9, pp. 2093–2104, 2013, doi: 10.1109/JPROC.2012.2221071.

[12] A. Insausti-Delgado, E. López-Larraz, J. Omedes, and A. Ramos-Murguialday, "Intensity and Dose of Neuromuscular Electrical Stimulation Influence Sensorimotor Cortical Excitability," *Front. Neurosci.*, vol. 14, p. 593360, 2020, doi: 10.3389/fnins.2020.593360.

[13] H. Wang *et al.,* "User Participatory Design of a Wearable Focal Vibration Device for Home-Based Stroke Rehabilitation," *Sensors*, vol. 22, no. 9, p. 3308, 2022, doi: 10.3390/s22093308.

[14] C. E. Seim, S. L. Wolf, and T. E. Starner, "Wearable vibrotactile stimulation for upper extremity rehabilitation in chronic stroke: clinical feasibility trial using the VTS Glove," *J. NeuroEng. Rehabil.*, vol. 18, no. 1, 2021, doi: 10.1186/s12984-021-00813-7.

[15] L. Lin *et al.,* "Comparison of Immediate Neuromodulatory Effects between Focal

Vibratory and Electrical Sensory Stimulations after Stroke," *Bioengineering*, vol. 11, no. 3, p. 286, 2024, doi: 10.3390/bioengineering11030286.
[16] V. Latora and M. Marchiori, "Efficient behavior of small-world networks," *Physical review letters*, vol. 87, no. 19, p. 198701, 2001.
[17] S. Zhou *et al.,* "Impairments of cortico-cortical connectivity in fine tactile sensation after stroke," *J. NeuroEng. Rehabil.*, vol. 18, no. 1, p. 34, 2021, doi: 10.1186/s12984-021-00821-7.
[18] F. de Vico Fallani *et al.,* "Multiscale topological properties of functional brain networks during motor imagery after stroke," *NeuroImage*, vol. 83, pp. 438–449, 2013, doi: 10.1016/j.neuroimage.2013.06.039.
[19] M. Rubinov and O. Sporns, "Complex network measures of brain connectivity: uses and interpretations," *NeuroImage*, vol. 52, no. 3, pp. 1059–1069, 2010, doi: 10.1016/j.neuroimage.2009.10.003.
[20] Z. Hao *et al.,* "CAMBA framework: Unveiling the brain asymmetry alterations and longitudinal changes after stroke using resting-state EEG," *NeuroImage*, vol. 282, p. 120405, 2023, doi: 10.1016/j.neuroimage.2023.120405.
[21] J. Faskowitz, F. Z. Esfahlani, Y. Jo, O. Sporns, and R. F. Betzel, "Edge-centric functional network representations of human cerebral cortex reveal overlapping system-level architecture," *Nat. Neurosci.*, vol. 23, no. 12, pp. 1644–1654, 2020, doi: 10.1038/s41593-020-00719-y.
[22] Y. Jo, F. Zamani Esfahlani, J. Faskowitz, E. J. Chumin, O. Sporns, and R. F. Betzel, "The diversity and multiplexity of edge communities within and between brain systems," *Cell reports*, vol. 37, no. 7, p. 110032, 2021, doi: 10.1016/j.celrep.2021.110032.